SYNTHESIS OF A HELICOPTER CONTROL SYSTEM USING INVERSE DYNAMICS AND ITS UPGRADE WITH THE USE OF A SIDESTICK CONTROLLER

Aleksandr V. Efremov[1] pvl@mai.ru
Eugene V. Efremov[1] pvl@mai.ru
Zoe Mbikayi[1] pvl@mai.ru
Sergey Yu. Esaulov[2] sergey_esaulov@bk.ru
Valery A. Ivchin[2] vivchin@mi-helicopter.ru
Maxim I. Myasnikov[2] mmyasnikov@mi-helicopter.ru

[1]Moscow Aviation Institute (RU), [2]Mil Kamov National Helicopter Center (RU)

Abstract

The modern trend of developing highly automated aircraft is characterized by a transition from traditional methods and technical solutions to innovative approaches of creating control systems, inceptors and displays. This paper deals with the development of helicopter control systems based on the inverse dynamics and its integration with a novel type of side stick shaping the pilot output signal such that it is proportional to the control force (Force Sensing Control – FSC). The synergetic asset arising from this integration is also evaluated. The evaluation of the effectiveness of the inverse dynamics was carried out through mathematical modeling of the pilot-aircraft system ground based simulations.

1. INTRODUCTION

The inverse dynamics technique is one of several techniques developed in the recent years that allow to change the dynamics of the aircraft considerably, making the control problem easier to solve.

It can be used as a nonlinear control technique based on feedback linearization or in the feedforward control loop. It has been used over the years for a variety of applications both for the fixed-wing airplane [1] and for the rotorcraft [2].

The main issue when using the inverse dynamics is the lack of robustness, as it requires exact mathematical models of the plant or those of processes affecting the plant, such as winds and disturbances. In [3] and [4], the author established bounds on plant uncertainties that would be acceptable when using the inverse dynamics. The method developed in [3] allows to use the inverse dynamics only when these bounds are respected. This makes the technique applicable only to a limited number of control problems.

As a nonlinear control technique, the inverse dynamics is used to make an appropriate coordinate transformation of the nonlinear plant [5], so that any linear control technique can be applied on the resulting linear plant. This is illustrated in [2] and [6] where the nonlinear dynamics inversion is used in the inner loop and a PID-type controller is used in the outer loop to achieve robustness to modeling uncertainties and disturbances. The same approach is used in [7], but the robustness is provided by an H-infinity-based controller in the outer control loop.

As a linear control technique, the inverse dynamics has mostly been used in the feedforward control loop to support feedback controllers. In this form, its integration with reference model techniques has been studied in [8]. Here, the desired dynamics from the pilot stick commands are computed via the use of reference models, which are then given to the inverse dynamics in order to compute the actuators positions necessary to achieve those desired dynamics.

This method however, still requires an exact model of the aircraft to be controlled. Therefore, a PID - type compensator must be added in order to provide robustness to modeling uncertainties and disturbances as in [2].

The inverse dynamics as a linear control method has also been used in [9] to decouple the dynamics of the plant and achieve good tracking performances, and the robustness is provided by a reference model and its inverse. This method however uses several loops in the control algorithm, making it difficult and expensive to implement.

This paper presents a method in which, a PI controller is used to provide robustness to the controlled element. And inverse dynamics are computed such that the inverse of the dynamics of the PI controller is taken into account. This approach allows it to effectively suppress the dynamics of the plant and the additional controller,

Presented at 46th European Rotorcraft Forum, Moscow, Russia, 8-11 September, 2020
This work is licensed under the Creative Commons Attribution International License (CC BY). Copyright © 2020 by author(s).

therefore improving the tracking performances and decoupling the dynamics.

Different inceptors and types of pilot output signal were investigated with the goal to define the best way of their integration with the inverse dynamics

2. MOTIVATION

The control systems algorithms are constructed following the inverse dynamics method on a linearized helicopter mathematical model as shown in figure 1.

The inverse dynamics are used in the feedforward loop to improve the tracking performances, and require a stable system [10]. The stability is therefore provided by a set of feedback gains.

The use of inverse dynamics is motivated by the reasoning shown in equations (1) and (2).

To achieve zero tracking error for a given reference signal *r(s)* or pilot command δ_e in a controllable and stable system *G(s)* as given in figure 1, the control signal *u(s)* can be computed as:

$$(1) \qquad \dot{y}(j\omega) = \delta_e(j\omega) = u(j\omega)\cdot G(j\omega)$$

$$(2) \qquad u(j\omega) = \frac{\delta_e(j\omega)}{G(j\omega)} = \delta_e(j\omega)\cdot G^{-1}(j\omega)$$

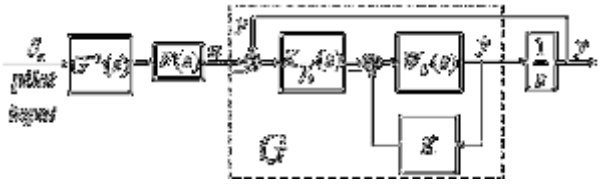


Figure 1. Using the inverse dynamics

where $G^{-1}(s)$ is the inverse dynamics and $\dot{y}$ is the vector of angular rates and climb rate $[q, p, r, w]$.

The proposed algorithms bring the frequency response $\frac{\dot{y}(j\omega)}{\delta_e(j\omega)}$ closer to a gain coefficient response in a wide frequency range and decouple control channels.

When the controlled element dynamics are $\frac{y(j\omega)}{\delta_e(j\omega)}$, the frequency response is then close to the integral. The frequency response characteristics of this process can be seen in figure 2 where the longitudinal dynamics of the helicopter equipped with feedback controllers are compared to the same dynamics equipped with the inverse dynamics controllers. Such type of dynamics guarantees the proportional type of pilot behavior.

It is worth noting that the dynamics used include a nonlinear actuator with rate limits ($\dot{\delta}_e = 30$ deg/sec) and a time delay of 0.2 seconds.

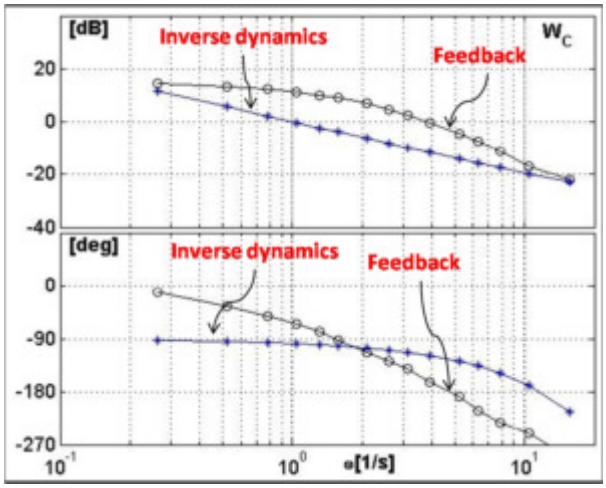


Figure 2. Inverse dynamics vs. feedback

3. COMPUTING THE INVERSE DYNAMICS

The inverse dynamics are computed analytically, following the technique given in [10].

The system G contains nonlinear elements as shown in the previous section. Therefore it needs to be linearized and represented in the state space form before computing the inverse dynamics. This is done using the Jacobian linearization method given in [11].

The system G with input u and output $\dot{y}$ is shown in figure 1. For simplicity, the output $\dot{y}$ will be denoted as capital *Y* in the rest of this paper.

The system G can be represented as a function of the input vector u and state vector x such that:

$$(3) \qquad \dot{x} = f(x,u)$$

with a vector of initial conditions $x(t_0) = x_0$ and equilibrium points consisting of a vector of nominal inputs $\bar{u}(t)$ corresponding to a vector of nominal state $\bar{x}(t)$ such that $\dot{\bar{x}} = f(\bar{x},\bar{u})$ and $\bar{x}(t_0) = x_0$.

Presented at 46th European Rotorcraft Forum, Moscow, Russia, 8-11 September, 2020
This work is licensed under the Creative Commons Attribution International License (CC BY). Copyright © 2020 by author(s).

Since the helicopter model W_C is linear itself, the initial conditions and equilibrium points are all taken at 0.

Now, suppose a perturbation is added in the input u that creates a perturbation in the state x such that:

$$\delta_x(t) = x(t) - \overline{x} \quad (4)$$

$$\delta_u(t) = u(t) - \overline{u} \quad (5)$$

If (4) and (5) are substituted in (3), it becomes:

$$\dot{\delta}_x = f(\overline{x} + \delta_x, \overline{u} + \delta_u) \quad (6)$$

Then a Taylor series expansion is performed on equation (6), and an approximation is made, which consists in assuming that all the terms of order higher than 1 are equal to 0.

Knowing that $f(\overline{x}, \overline{u}) = 0$, (5) becomes:

$$\dot{\delta}_x(t) \approx \left.\frac{\delta_f}{\delta_x}\right|_{(\overline{x},\overline{u})} \delta_x(\mathrm{t}) + \left.\frac{\delta_f}{\delta_u}\right|_{(\overline{x},\overline{u})} \delta_u(\mathrm{t}) \quad (7)$$

From (7), matrices A and B of the state space representation of the system G can be extracted by applying (8).

$$\dot{\delta}_x(t) = A\delta_x(t) + B\delta_u(t) \quad (8)$$

Using the matrices A and B obtained above, the state space representation can be constructed as shown by (9) and (10).

$$\mathrm{sX(s)} = \mathrm{AX(s)} + \mathrm{BU(s)} \quad (9)$$

$$\mathrm{Y(s)} = \mathrm{CX(s)} \quad (10)$$

where X is the state vector, U is the input vector and *C* is the matrix relating the state vector *X* to the output vector *Y* of the system *G*.

The transfer function representation can then be derived by re-writing (9) in terms of X(s) as shown in (11), and replacing it in (10) as to obtain equation (12):

$$\mathrm{X(s)} = (\mathrm{sI - A})^{-1} \cdot \mathrm{BU(s)} \quad (11)$$

$$\mathrm{Y(s)} = \mathrm{C}\ (\mathrm{sI - A})^{-1} \cdot \mathrm{BU(s)} \quad (12)$$

The relationship between the state space representation and the transfer functions can then be written as:

$$\frac{Y(s)}{U(\mathrm{s})} = \mathrm{C}\ (\mathrm{sI - A})^{-1} \cdot \mathrm{B} \quad (13)$$

This will result in a matrix of transfer functions that can be inverted individually such that for a transfer function $G(s) = \frac{y(\mathrm{s})}{\mathrm{u(s)}}$ the inverse dynamics is given by $G^{-1}(s) = \frac{\mathrm{u(s)}}{\mathrm{y(s)}}$.

It is worth noting that equation (13) is valid only if

the number of rows of matrix *C* is equal to the number of columns of matrix *B*. This means the number of inputs of the system should be equal to the number of outputs, such that each input controls an individual output.

4. ISSUES WITH INVERSE DYNAMICS

As much as the inverse dynamics technique is attractive because of its tracking performances and coupling cancellation, it presents some issues. The two main issues evaluated in this paper are the fact that the inverse dynamics transfer functions are improper for most real life systems, and the lack of robustness.

4.1. Propening filters

The helicopter transfer functions are proper or strictly proper. This implies that the inverse dynamics would have numerators of a higher order than the denominators.

$$G^{-1}(s) = \frac{b_m s^m + \cdots}{a_n s^n + \cdots}$$

where *m* > *n.*

This issue is solved by introducing propening filters *F(s)* that make the inverse dynamics proper as it can be seen on figure 1. This will equalize the order of the numerators and denominators of the inverse dynamics.

The frequencies of the filters are chosen to be high enough as not to have a considerable impact on the inverse dynamics, and low enough as to not saturate the actuators. The filters therefore also allow to make a tradeoff between the control cost and performances.

4.2. Robustness

Another main issue when using the inverse dynamics technique is that it requires a precise mathematical model of the plant.

PI controllers given by $K_{1/s}(s) = K_s \frac{Ts+1}{s}$ are introduced in order to add robustness to the system.

The PI controllers are implemented as shown in figure 1. This structure allows the controllers to

Presented at 46th European Rotorcraft Forum, Moscow, Russia, 8-11 September, 2020
This work is licensed under the Creative Commons Attribution International License (CC BY). Copyright © 2020 by author(s).

asymptotically minimize the attitude error, which can be considered as a representation of the uncertainties in the model.

5. RESEARCH PLAN

The effectiveness of inverse dynamics was studied using ground based simulations and mathematical modeling of the pilot aircraft system.

5.1. Mathematical modeling of the pilot-aircraft system

The modified pilot-structural model (modified Hess' pilot model) developed in [12] and shown on figure 3 was used for the mathematical modeling investigations.

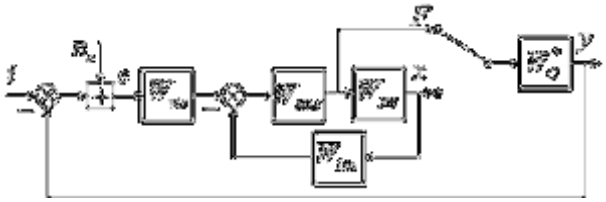


Figure 3. Modified pilot structural model

Here:

$W_{vis} = K_L \dfrac{T_L j\omega + 1}{T_I j\omega + 1} e^{-\tau j\omega}$ is the model of perception and compensation of visual information;

$W_{kin} = \dfrac{K_n (j\omega)^2}{T_n^2 (j\omega)^2 + 2T_n (j\omega) + 1}$ is the model of perception and compensation of proprioceptive information;

$W_{NM} = \dfrac{1}{(T_{N^*} j\omega + 1)} \dfrac{1}{(T_N^2 (j\omega)^2 + 2\zeta_N j\omega + 1)}$ is the neuromuscular system model;

$W_{FS} = \dfrac{K_{FS}}{(j\omega)^2 + 2\zeta_{FS}\omega_{FS} j\omega + \omega_{FS}^2}$ is the model of the inceptor;

n_e is the pilot noise (remnant) characterized by the spectral density $S_{n_e n_e} = K_{n_e} \pi \dfrac{\sigma_e^2 + T_L^2 \sigma_{\dot{e}}^2}{1 + T_L^2 \omega^2}$, where σ_e^2 and $\sigma_{\dot{e}}^2$ are the variances of error and its derivative, $K_{n_e} = 0.01$,

W_C^* is the controlled element dynamics which is the mathematical model of the vehicle and the flight control system dynamics. The vector of parameters of the structural model $a = (T_{L,} K_{L,} T_{n,} K_n)$ is computed by running the minimization criterion $I = \min\ \sigma_e^2$ where the variance of error σ_e^2 is determined by the equation given in [13] as:

$$\sigma_e^2 = \frac{\sigma_{ei}^2 (1 - \mathrm{K}_{n_{\dot{e}}} \mathrm{T}_L{}^2 \mathrm{B}_m) + \sigma_{\dot{e}_i}^2 \mathrm{K}_{n_{\dot{e}}} \mathrm{T}_L{}^2 A_m}{1 - \mathrm{K}_{n_e} A_m - \mathrm{K}_{n_{\dot{e}}} \mathrm{T}_L{}^2 B_m}$$

Where:

$$A_m = \int_{-\infty}^{\infty} \frac{|\Phi|^2}{1 + T_L{}^2 \omega^2} d\omega \ ; \ B_m = \int_{-\infty}^{\infty} \frac{|\Phi|^2 \omega^2}{1 + T_L{}^2 \omega^2} d\omega$$

$$\sigma_{e_i}^2 = \int_0^{\infty} S_{e_i e_i}(\omega)\, \mathrm{d}\omega \ ; \ \sigma_{\dot{e}_i}^2 = \int_0^{\infty} \omega^2 S_{e_i e_i}(\omega)\, \mathrm{d}\omega$$

$$S_{e_i e_i}(\omega) = |\Phi_e(\mathrm{j}\omega)|^2 \ S_{ii}(\omega) \ ; \ \Phi_e(\mathrm{j}\omega) = \frac{E(\mathrm{j}\omega)}{I(\mathrm{j}\omega)}$$

$S_{ii}(\omega)$ is the spectral density of the input signal, $\Phi(\mathrm{j}\omega)$ is the closed loop system describing function.

The structural model shown in figure 3 allows to study the pilot aircraft system for two types of pilot output signal. One of them is the displacement, realizing the so-called "Displacement Sensing Control (DSC)", and the other one is the force applied by the pilot, realizing the so-called "Force Sensing Control (FSC)" [14].

5.2. Ground based simulations

The effectiveness of the inverse dynamics was also studied using the ground based simulator equipped with a collimator visual system and the MOOG control loading system (see figure 4).

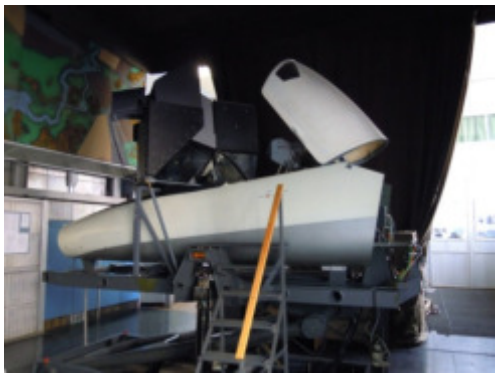


Figure 4. Ground based simulator

The image of the compensatory display was shown on the screen of the central collimator. The vertical motion of the symbol on this display allowed to realize the compensatory pitch tracking task.

Presented at 46th European Rotorcraft Forum, Moscow, Russia, 8-11 September, 2020
This work is licensed under the Creative Commons Attribution International License (CC BY). Copyright © 2020 by author(s).

The MOOG system equipped with the force and displacement sensors allowed to evaluate the effectiveness of the DSC and FSC types of pilot output.

Two operators and one licensed pilot were involved in the experiments. They all have sufficient experience in ground based simulations.

The compensatory pitch tracking task was carried out with a polyharmonic input signal $i(t) = \sum_{k=1}^{15} A_k \cos \omega_k t$ which appeared as a random signal to the operators. Its amplitude A_k and orthogonal frequencies $\omega_k = K\frac{2\pi}{T}$,where T is the duration of trials, were selected from requirements of correspondence between the power distributions of the polyharmonic signal and a random signal characterized by the spectral density $S_{ii} = \frac{K^2}{(\omega^2 + 0.5^2)^2}, \sigma_i^2 = 4\,cm^2$.

The Fourier coefficient technique [15] was used for the computation of the main pilot-vehicle system characteristics:

- Pilot $W_p(\mathrm{j}\omega)$, open-loop $W_{OL}(\mathrm{j}\omega)$ and closed-loop $\Phi(\mathrm{j}\omega)$ describing functions.
- Pilot remnant spectral density $S_{n_e n_e}(\omega)$.
- Variance of error σ_e^2 and its components $\sigma_{e_i}^2$ which is the variance of error correlated with the input signal and $\sigma_{e_n}^2$ which is the variance of error correlated with the remnant.

The experiments were carried out with the central and side sticks.

The following controlled element dynamics W_C^* were used during the experiments:

$W_C^* = W_{fb}$: The controlled element dynamics of the vehicle equipped with the feedback control system only.

$W_C^* = W_{inv}$: The controlled element dynamics of the vehicle equipped with the feedback control system and inverse dynamics whose parameters correspond to the exact model of the vehicle.

$W_C^* = \tilde{W}_{inv}$: The controlled element dynamics of the vehicle equipped with the feedback control system and the inverse dynamics whose parameters exhibit uncertainties in the model of the vehicle. The uncertainties were simulated by reducing the elements of the state matrix A to 75% of their nominal values, and the input matrix B to 50%.

$W_C^* = \tilde{W}_{inv+PI}$: The controlled element dynamics of the vehicle equipped with the feedback control system, the inverse dynamics and a PI controller. The parameters of the PI controller were selected such that they approximate the frequency response characteristics of $W_C^* = \tilde{W}_{inv+PI}$ to $W_C^* = W_{inv}$.

At least 3 trials were executed for each variable (controlled element dynamics, type of inceptor and pilot's output) and the results of identification were averaged. The duration of each trial was equal to 144 s.

6. RESULTS OF THE INVESTIGATION

The results of the ground based simulation carried out for two types of flight control system based on the use of traditional feedbacks only ($W_C^* = W_{fb}$) and inverse dynamics principle ($W_C^* = W_{inv}$) are shown in figure 5.

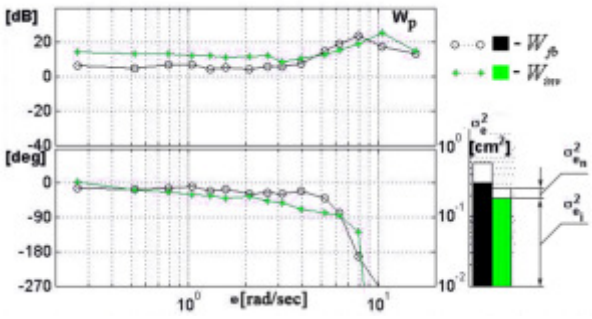


Figure 5. Results of experiments

It is seen that when the inverse dynamics is used, the variance of error σ_e^2 is 2.3 times less with a lower pilot lead phase compensation in the middle frequency range.

Qualitatively, close results were obtained in the mathematical modeling as well (see figure 6).

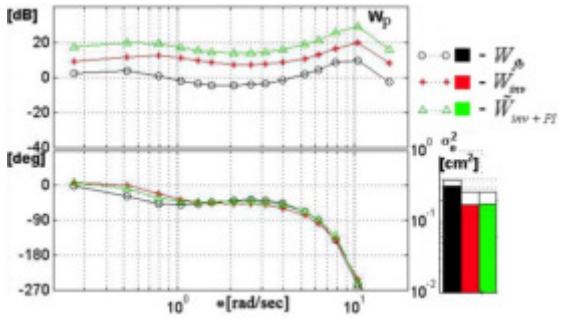


Figure 6. Results of mathematical modeling

Presented at 46th European Rotorcraft Forum, Moscow, Russia, 8-11 September, 2020
This work is licensed under the Creative Commons Attribution International License (CC BY). Copyright © 2020 by author(s).

In the case when the controlled element dynamics corresponds to $W_C^* = \tilde{W}_{inv}$, the effectiveness of the inverse dynamics decreases considerably which causes the variance of error σ_e^2 to increase 1.5 times compared to when the dynamics correspond to $W_C^* = W_{inv}$ (the controlled element dynamics of the vehicle equipped with the feedback control system and inverse dynamics whose parameters correspond to the exact model of the vehicle).

The installation of the PI controller in the flight control system based on the use of inverse dynamics allowing to transform the dynamics into $W_C^* = \tilde{W}_{inv+PI}$ leads to a considerable improvement of the accuracy compared to the case when the mathematical modeling investigation was carried out with $W_C^* = W_{fb}$ (see figure 6). And the variance of error σ_e^2 is then practically the same as the one obtained in the experiment with the dynamics $W_C^* = W_{inv}$.

Both the pilot describing function and the frequency response characteristics of the closed loop system were calculated. This allowed to compute the parameters of the so-called "MAI new criterion for flying qualities prediction" [16].

The parameters of this criterion are the following:

- The bandwidth of the closed loop system (ω_{BW}) corresponding the frequency at which the phase frequency characteristics of the closed loop system is equal to -90 deg.
- The pilot compensation parameter ($\Delta\varphi_{\max}$) calculated in the all frequency range as the maximal difference between the pilot phase characteristics of the investigated dynamics and those of the dynamics which do not require any pilot phase compensation (phase characteristics corresponding to a time delay element).

The values of these parameters, calculated through mathematical modeling of the pilot-aircraft system in the hovering task for two controlled element dynamics ($W_C^* = W_{fb}, W_C^* = W_{inv}, W_C^* = \tilde{W}_{inv}$, $W_C^* = \tilde{W}_{inv+PI}$,), are given in figure 7.

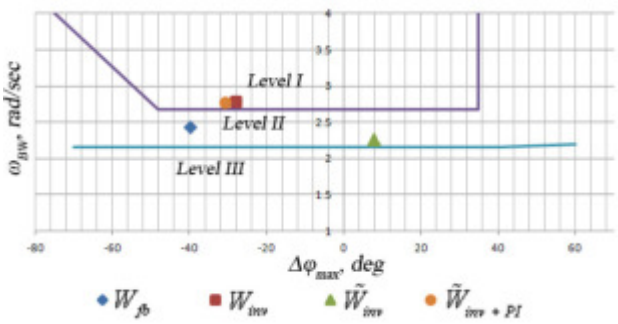


Figure 7. MAI New criterion

The results shown in figure 7 demonstrate that the use of the inverse dynamics $W_C^* = W_{inv}$ or $W_C^* = \tilde{W}_{inv+PI}$ allows to improve the flying qualities, making them correspond to the 1st level.

In the case when the control system is based on the feedbacks only or when $W_C^* = \tilde{W}_{inv}$, the flying qualities belong to the 2nd level.

The evaluation of the flying qualities using the Bandwidth/ Time Delay criterion from ADS-33E-RPF for the same dynamics did not expose the fact that the all investigated dynamics belong to different levels.

A set of experiment was executed to evaluate the effectiveness of the inverse dynamics with different types of inceptors (central and side sticks) on the pilot-aircraft system characteristics. The research demonstrated that for both the central and side sticks, the pilot lead compensation is lower for the DSC type of pilot output. As an example, figure 8 demonstrates the pilot frequency response characteristics obtained for the side stick with both the DSC and FSC types of pilot output.

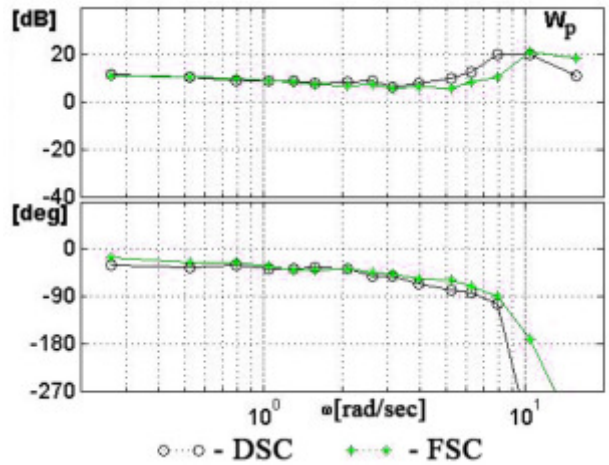


Figure 8. Pilot describing functions for DSC and FSC pilot outputs

Besides this, the use of a side stick demonstrated a decrease of variance of error σ_e^2 for the case when

Presented at 46th European Rotorcraft Forum, Moscow, Russia, 8-11 September, 2020
This work is licensed under the Creative Commons Attribution International License (CC BY). Copyright © 2020 by author(s).

the DSC type of pilot output and traditional type of flight control system ($W_C^* = W_{fb}$) were used.

For different operators (operator A and B), the variance of error σ_e^2 decreases by a factor of 1.1 to 1.3 (see figures 9 and 10). The same consistencies were obtained in [12] for different aircraft dynamics configurations.

The experiments executed for the inverse dynamics with the same type of inceptor and pilot output demonstrated a decrease of variance of error σ_e^2 by an additional factor of 1.8. When the FSC type of pilot output was used, the variance of error decreased even more, by a factor of 1.55. These results are shown on figures 9 and 10.

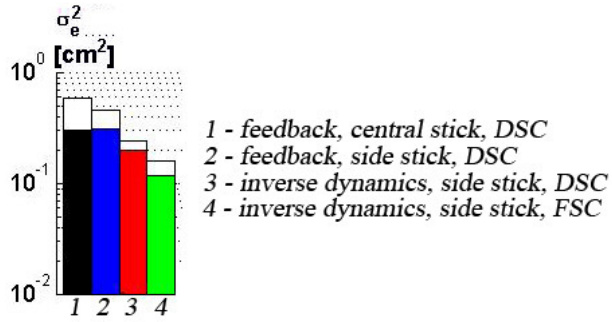


Figure 9. Variance of error (Operator A)

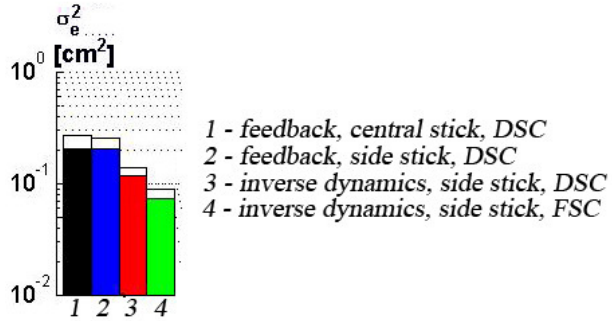


Figure 10. Variance of error (Operator B)

The influence of the inverse dynamics in combination with different types of inceptors and pilot output was not limited to the variance of error σ_e^2.

The results of their influence on other pilot and pilot-aircraft system characteristics are given in tables 1 and 2.

Table 1. Results of experimental investigations (Operator A).

stick	Parameter	Feedback		Inverse dynamics	
		Central stick	Side stick	Central stick	Side stick
DSC	σ_e^2, cm^2	0.59	0.46	0.26	0.24
	ω_c, rad/ sec	2.81	2.51	2.85	2.84
	ω_{BW}, rad/ sec	2.94	2.70	3.01	3.00
FSC	σ_e^2, cm^2	0.44	0.22	0.19	0.16
	ω_c, rad/ sec	2.85	2.95	3.03	3.11
	ω_{BW}, rad/ sec	3.06	2.99	3.38	3.59
	$\Delta\varphi\|_{\omega=10\,\text{rad/sec}}$, deg	23.1	200.6	33.7	82.4

Table 2. Results of experimental investigations (Operator B).

stick	Parameter	Feedback		Inverse dynamics	
		Central stick	Side stick	Central stick	Side stick
DSC	σ_e^2, cm^2	0.27	0.25	0.15	0.14
	ω_c, rad/ sec	2.97	2.70	2.97	3.02
	ω_{BW}, rad/ sec	3.23	2.99	3.48	3.56
FSC	σ_e^2, cm^2	0.21	0.14	0.10	0.09
	ω_c, rad/ sec	2.99	3.23	3.14	4.05
	ω_{BW}, rad/ sec	3.14	3.73	4.06	4.44
	$\Delta\varphi\|_{\omega=10\,\text{rad/sec}}$, deg	31.9	168.9	5.2	77.4

Here:

ω_c is the crossover frequency of the open loop system;

ω_{BW} is the bandwidth frequency of the closed loop system;

Presented at 46th European Rotorcraft Forum, Moscow, Russia, 8-11 September, 2020
This work is licensed under the Creative Commons Attribution International License (CC BY). Copyright © 2020 by author(s).

$\Delta\varphi\big|_{\omega=10}$ is the difference between pilot phase frequency response characteristics obtained in experiments with DSC and FSC type of pilot output.

It is seen that the transition from the traditional central stick to the side stick with DSC type of pilot output is accompanied by an increase of crossover frequency ω_c and bandwidth ω_{BW}.

And the transition from DSC to FSC type of pilot output is accompanied by an additional increase of these parameters and a decrease of the pilot phase delay $\Delta\varphi\big|_{\omega=10}$ in the high frequency range.

7. CONCLUSION

A control technique was developed by combining the inverse dynamics with the fight control system based on the use of feedbacks only.

The realization of the inverse dynamics and necessity of robustness required the installation of proper filters and PI controllers in the flight control system.

Experimental investigations demonstrated the high efficiency of the inverse dynamics. Its integration with the side stick and force sensing control type of pilot output allowed to decrease the variance of error by a factor of 3 to 3.9 in comparison to the traditional helicopter control system with feedbacks, central stick and DSC type of pilot output. It allowed to decrease the pilot phase delay in the high frequency range as well.

8. REFERENCES

[1] Padhi R., Rao P. N., Goyal S. and Balakrishnan S. N. “Command tracking in high performance aircrafts: A new dynamic inversion design.” IFAC Proc. 4 (7), 2007. doi:10.3182/20070625-5-FR-2916.00015

[2] Horn J. F. Non-Linear Dynamic Inversion Control Design for Rotorcraft. Journal Aerospace 6(3) 38, 2019. doi:10.3390/aerospace6030038

[3] S. Devasia. Robust inversion-based feedforward controllers for output tracking under plant uncertainty. Proc. of the 2000 American Control Conference, vol. 1, pp. 497-502, 2000. doi:10.1109/ACC.2000.878950

[4] S. Devasia. Should model-based inverse inputs be used as feedforward under plant uncertainty?. IEEE Trans. on Aut. Control, Vol.45, no. 11, pp. 1865-1871, 2002. doi:10.1109/TAC.2002.804478

[5] J. S. Brinker and K. A. Wise. Stability and flying qualities robustness of a dynamics inversion aircraft control law. Journal of Guidance, Control and Dynamics, Vol. 19, No. 6, November-December 1996. doi:10.2514/3.21782

[6] Ansari U. and Bajodah A. H. Robust generalized dynamic inversion based-control of autonomous underwater vehicles. Proc. of the Institution of Mechanical Engineers, Part M: Journal of Engineering for the Maritime Environment 232(4) p434, 2018. doi:10.1177/1475090217708640

[7] Peng C., Han C., Zou J. and Zhang G. H-infinity Optimal Inversion Feedforward and Robust Feedback Based 2DOF Control Approach for High Speed-Precision Positioning Systems. Journal of Control Science and Engineering, Article ID 7256039, 2016. doi:10.1155/2016/7256039

[8] Miller C. J. Nonlinear Dynamic Inversion Baseline Control Law: Architecture and Performance Prediction. Proc. of the 2011 AIAA Conf. Guidance, Navigation and Control(Portland, OR, USA), 2011. doi:10.2514/6.2011-6467

[9] Z Mbikayi, A V Efremov and E V Efremov. Integration of the inverse dynamics with a reference model technique, and its application for the improvement of the helicopter flying qualities. IOP Conf. Ser.: Mater. Sci. Eng. 868 012016, 2020. doi:10.1088/1757-899X/868/1/012016

[10] Buchholz J. J. and Von Grunhagen W. Inversion Impossible?. Tech. Rep., Bremen university of Applied Sciences and DLR Braunschweig, Germany, 2008. http://www.buchholz.hs-bremen.de/inversion/inversion_impossible.pdf

[11] Andrew Packard, Kameshwar Poolla, Roberto Horowitz. Dynamic Systems and Feedback. Class Notes for ME 132. Department of Mechanical Engineering, University of California. 2002. https://www.cds.caltech.edu/~murray/courses/cds101/fa02/caltech/pph.html

[12] A. V. Efremov, V. V. Aleksandrov, E. E. Efremov, M. V. Vukolov. The influence of different types of inceptors and their characteristics on pilot-aircraft system. 2nd IFAC Conference on Cyber-Physical & Human systems, Miami, Florida, USA, Dec. 2018. doi:10.1016/j.ifacol.2019.01.013

[13] Efremov A. V. Pilot-Aircraft system. Regularities and mathematical models of pilot behavior. pp. 1-193 MAI 2017.

[14] David H. Klyde and Duane McRuer. Smart-Cue and Smart-Gain concepts development to alleviate loss of control. Journal of Guidance, Control and Dynamics Vol. 32, No. 5, Sep-Oct 2009. doi:10.2514/1.43156

Presented at 46th European Rotorcraft Forum, Moscow, Russia, 8-11 September, 2020

This work is licensed under the Creative Commons Attribution International License (CC BY). Copyright © 2020 by author(s).

[15] Efremov A. V. et. al. Investigation of pilot induced oscillation tendency and prediction criteria development. WL-TR-96-3109 Wright laboratory pp. 1-138, USA May 1996.

[16] Efremov A. V., Efremov E. V. Tiaglik, M. S. Advancements in predictions of flying qualities, pilot-induced oscillation tendencies, and flight safety. Journal of Guidance, Control and Dynamics Vol. 43, No. 1, 2020. doi:10.2514/1.G004409

Presented at 46th European Rotorcraft Forum, Moscow, Russia, 8-11 September, 2020

This work is licensed under the Creative Commons Attribution International License (CC BY). Copyright © 2020 by author(s).